LEIDENFROST RATCHETS

by

MIKE TAORMINA

A THESIS

Presented to the Department of Physics
and the Honors College of the University of Oregon
in partial fulfillment of the requirements
for the degree of
Bachelor of Science

June 10, 2006

An Abstract of the Thesis of

Michael James Taormina for the degree of Bachelor of Science

in the Department of Physics to be taken June 2006

Title: LEIDENFROST RATCHETS

Approved: _____

Dr. Heiner Linke

A "Leidenfrost ratchet" is a device which facilitates a newly-discovered phenomenon, where drops of liquid accelerate across a heated substrate. The system has been qualitatively studied and a vapor flow model has been suggested to account for this observed behavior. This paper provides a study of general behavior, considerations needed to apply and test a vapor flow model for the ratchet system, and submits the model to an experimental trial. The results show the quantitative validity of a vapor flow model, while exposing subtle qualitative inconsistencies for the behavior of water and ethanol droplets. Content of the study can be used as a starting point for more detailed analysis of the system, possibly leading to novel scientific and industrial applications.

I would like to extend gratitude to the members of the Physics community at the UO. Specifically, to Heiner for the opportunity to join his research group. Also to Brian Long for intellectual discussions and Benji Alemán for his significant contributions to the project. Thanks as well to professor Schombert, who is likely responsible for pushing me into the study of physics.

Contents

Chapter 1

Introduction

1.1 The Leidenfrost Ratchet

When an amount of liquid is placed on a heated surface, it experiences evaporation at different rates depending on the surface temperature relative to the liquid's boiling point [1]. Above the boiling point, *nucleate boiling* begins, as pockets of gas develop along the heated surface of the liquid. As temperature is increased, the boiling becomes more violent, as these gas pockets form larger and more rapidly. This continues until a certain temperature, called the *Leidenfrost point* is reached. Above this temperature, vapor escapes the liquid rapidly enough to cause a pressure sufficient to support the entire weight of the liquid, which rests on top of the newly formed vapor layer (see figure 1.1). Thus, a small amount of liquid placed on a surface whose temperature is above the Leidenfrost point is completely separated from the surface by the vapor that is escaping the droplet itself. The film of vapor that supports the droplet also serves to insulate it, maximizing the lifetime of a boiling droplet.

This paper will study a phenomenon observed when film boiling (*Leidenfrost*) drops of liquid are placed on periodically asymmetric surfaces (*ratchets*). Namely, that such a droplet will experience a net force in a preferred direction relative to the ratchet surface (see figure 1.2 and website [2]). Said phenomenon represents a manifestation of

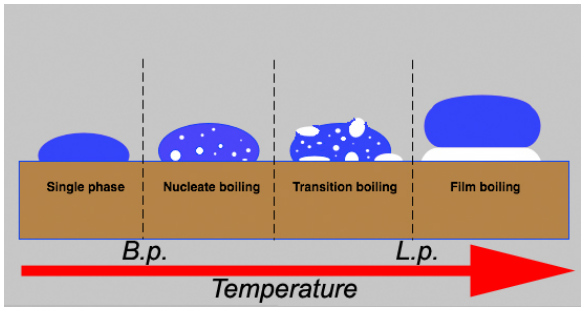

Figure 1.1: Different boiling regimes. Adapted from [18]

the "ratchet effect," where properties of asymmetry and disequilibrium are exploited to obtain useful work from an otherwise random physical system.

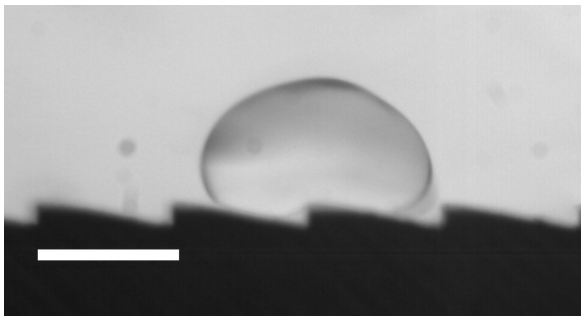

Figure 1.2: Film boiling nitrogen droplet on ratchet surface. In the image, the droplet would be observed as moving to the right. The scale bar length is 1.5mm. Ratchets are machined from brass or plastic, which are chosen for their compatibility with fabrication procedures. Plastic ratchets can be used for liquid nitrogen, which film boils at room temperature, while brass ratchets can be heated to temperatures sufficient for most common liquids to film boil.

Similar effects, where drops of liquid spring into directed motion along the surface of a substrate, have been demonstrated using a chemical [3, 4, 5, 6, 7, 8, 9], thermal [3, 10, 11], or electrical [12] gradient. The droplets in these systems typically must be in contact with the substrate surface and are therefore subject to wetting related forces. Resulting motion is usually limited to a few $\frac{mm}{s}$ and overall transport rarely exceeds a few centimeters. The system studied here is a unique alternative to these processes because of the formation of a thin layer of vapor between the liquid and

ratchet. This vapor layer serves as a low-friction surface over which the droplet can move faster and farther in comparison to other ratchet systems.

This effect was discovered by Matt Francis and Dr. Heiner Linke, and makes possible a new class of liquid transport devices with possible applications in both industrial and laboratory processes. It has been described in [13] and received attention in the scientific and popular media [14, 15]. The ratchet system possesses asymmetry as a spatial feature, machined into the ratchet geometry. A thermal gradient that is perpendicular to the direction of motion (the ratchet is heated from below) keeps the system out of thermal equilibrium. Spontaneous acceleration of droplets in this system has been observed for all liquids tested (boiling points ranging from $-196°C$ to $+151°C$) and is expected to occur for any liquid, provided the temperature is above the Leidenfrost point.

The system's behavior has been previously described by Laura Melling [16] and a preliminary model was developed by Benjamín Alemán in 2004 [17]. The basic concept of this model is that the droplet experiences a force due to vapor that is flowing beneath it. Therefore, it will be referred to throughout this paper as the *vapor flow model*. The course of my research that is represented here has been to build upon this previous work, gathering more complete data of droplet behavior, adapting the existing model into an experimentally testable form, and carrying out the preliminary experimental verification of the vapor flow model.

Chapter 2

Phenomenology

Before exploring the dynamic processes involved in droplet motion, I will first describe how film boiling droplets behave in the ratchet system and quantify some initial observations that have been made.

2.1 Kinematics

In order to experimentally characterize the force produced in the ratchet system, data will need to be taken of the acceleration experienced by the droplet. To accomplish this, I first note, as observed by Melling [16], that droplet motion is consistent with a differential equation which includes a constant (velocity independent) driving force (*ratchet force*) and a retarding force that is linear in velocity (*drag force*):

$$m\frac{d^2x}{dt^2} = F_{ratchet} - \beta\frac{dx}{dt} \tag{2.1}$$

Solving this equation, an expression for velocity is obtained:

$$v(t) = \left(v_0 - \frac{a}{\left(\frac{\beta}{m}\right)} \right) e^{-\frac{\beta}{m}t} - \frac{a}{\left(\frac{\beta}{m}\right)} \tag{2.2}$$

Here, m is the droplet mass, $\frac{d^2x}{dt^2}$ is the net acceleration experienced by the droplet, $F_{ratchet} \equiv ma$ is the driving ratchet force, a is the acceleration resulting from the ratchet force, β is the drag coefficient, $\frac{dx}{dt} \equiv v$ is the velocity of the droplet, and t is time. By experimentally measuring the velocity profile of a droplet in the ratchet system, equation 2.2 can be fit to the data and used to determine values for a and $\frac{\beta}{m}$. Experimental data of droplet velocity matches this fit equation quite well for droplets in the film boiling regime, as shown in figure 2.1. As will be discussed in section 2.2, data fit the curve, but show more fluctuation in velocity at lower temperatures. Experimental and data analysis procedures are given in appendix A.

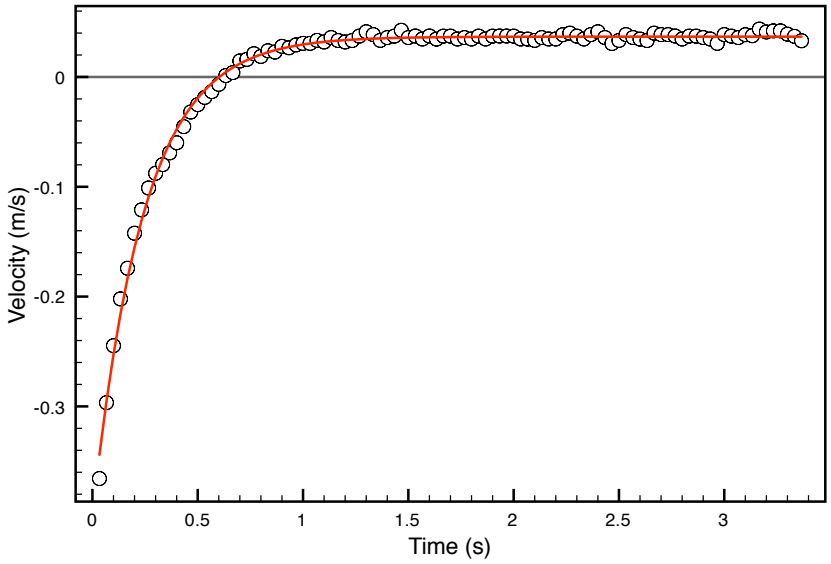

Figure 2.1: A typical plot of the velocity of a film boiling droplet of R-134a (a common refrigerant, B.P. $\approx -26°C$) as a function of time. The droplet was given initial velocity opposing the preferred direction of motion and reverses direction under the influence of the ratchet force. This data was taken at a ratchet temperature of $70°C$. The circles represent a three point average of experimental data (see appendix A) and the curve is fit equation 2.2.

Since the physical value of acceleration in mathematically equivalent to the second time derivative of a particle's position, one may first attempt to calculate acceleration directly from position data. Under constant acceleration, the data could be fit to a simple parabolic curve $x(t) = \alpha t^2 + \beta$, where $a = \ddot{x}(t) = 2\alpha$ gives the desired quantity. Because of the presence of a drag term, however, the position data will *not* be simply parabolic, except near zero velocity when drag is small. To use a parabolic fit, it would be necessary to restrict oneself to the data gathered in the region near $v = 0$.

Fit equation 2.2 was observed to be experimentally preferable to a simple parabolic fit of position near the zero velocity region of droplet motion. In order to see why, consider the equivalent fit to velocity: a linear fit of the points around $v = 0$. As shown in figure 2.2, this type of fit is very sensitive to scatter in the experimental data. For a set of points, a number of different slopes appear feasible as accurate characterizations of the data depending on how many are included and the error in each point. Utilizing equation 2.2 allows the use of significantly more data points, improving fit accuracy and providing information about the drag constant $\frac{\beta}{m}$ and the terminal velocity achieved by the droplet.

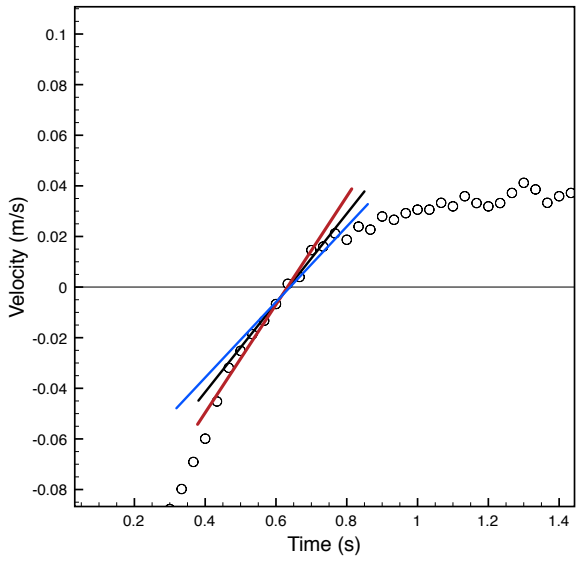

Figure 2.2: Linear fits of several different slopes seem plausible around the point where $v = 0$, making the use of such a fit undesirable to determine acceleration.

2.2 Temperature Dependence

Since the heat flow from ratchet to droplet is the driving energy source of droplet motion, it is a good idea to first study how the ratchet effect depends on temperature. In order to do this, I have gathered data for droplets of a fixed volume over a range of ratchet temperatures. This was done for three liquids: refrigerant R-134a, ethanol, and water. For the latter two, data acquisition began at the lowest temperature at which droplet motion was observed and the liquid was thought to be entering the film boiling temperature regime (the fact that film boiling may have only been partially achieved will be discussed in the following paragraphs where two different temperature regimes are identified). In the case of R-134a, this is already occurring at room temperature, so that is where experimental data begins.

Using the same experimental procedure as above, data for the acceleration and drag of droplets was gathered over a temperature range of about $200°C$. Of particular interest is the droplet acceleration as it depends on temperature, which is summarized for the three liquids in figure 2.3.

It is useful to distinguish two different temperature regimes from this data: I will therefore refer to the *low* and *high* temperature regimes, as indicated in figure 2.3. Droplets in the low temperature regime tend to experience the highest values for acceleration, but also show the most scatter in the data. Once in the high temperature regime, however, acceleration tends to become more stable and varies little with an increase in temperature. A difference in behavior can also be observed by comparing the velocity profile of a droplet in the low temperature regime with the previously shown data for a drop in the high temperature regime as shown in figure 2.4. While the *overall* behavior of the droplet in the low-temperature plot tends to follow equation 2.2, it is subject to fluctuations around the actual curve. Spontaneous acceleration and deceleration events can be seen as rapid increases and decreases in velocity.

We attribute this behavior to spontaneous nucleate boiling events, where the droplet briefly comes into contact with the ratchet surface, resulting in the type of violent boiling characteristic of the *transition boiling regime*. This may happen if the liquid is

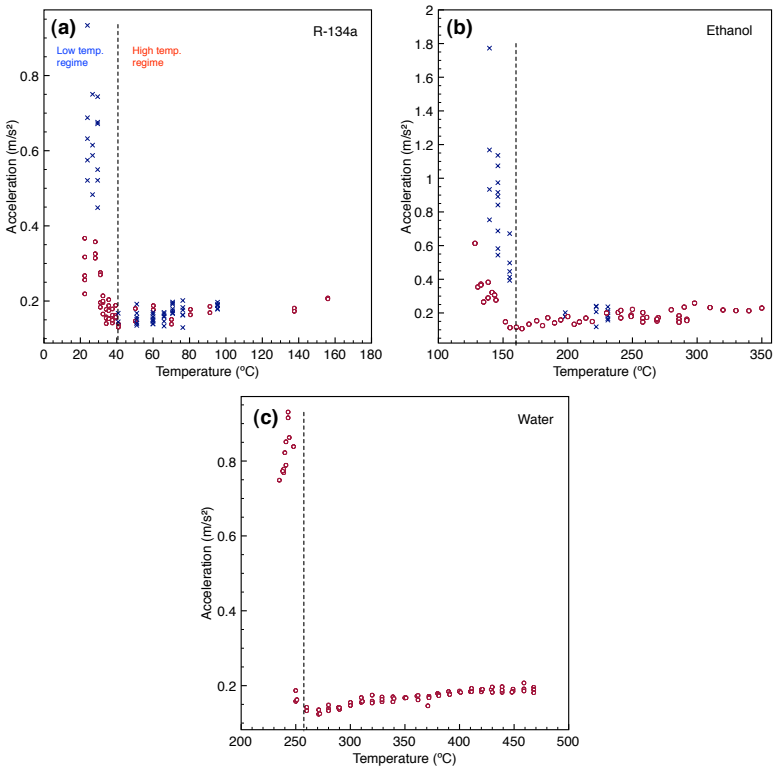

Figure 2.3: Acceleration measured by fitting equation 2.2 to experimental data for velocity. Crosses indicate cleaning the ratchet surface with brass polish only, while circles represent data obtained after additional cleaning by sonication (outlined in appendix A). The dashed line distinguishes two different temperature regimes, separated by scatter observed in droplet behavior.

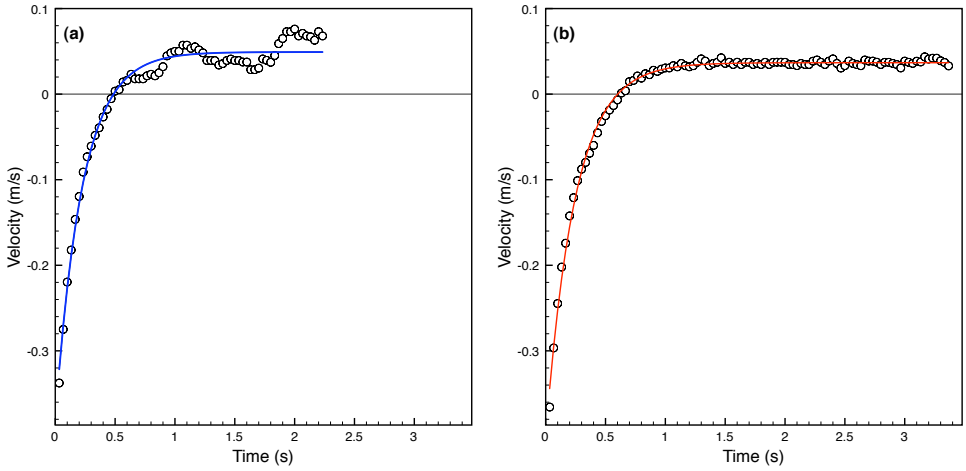

Figure 2.4: Velocity evolution of R-134a droplets in the low **(a)** and high **(b)** temperature regimes. Data was taken at temperatures of $22°C$ and $70°C$ respectively.

not yet entirely in the film boiling temperature range. This supposition is supported by the dependence on the cleaning method used. It is well known that the Leidenfrost point can vary substantially with surface roughness and cleanliness [18, 19]. In the low temperature regime, where the temperature may be near the Leidenfrost point, the cleaning method used substantially affects the observed acceleration, while in the high temperature regime, where liquid is presumably not in contact with the surface, cleaning doesn't notably impact droplet motion.

2.3 Ratchet Orientation and the Role of Gravity

A final observation of droplet behavior is made by replacing the horizontally-oriented ratchet with a channel having a flat bottom and ratcheted side walls (see figure 2.5).

A drop of film boiling liquid placed in such a channel experiences a net force in the same direction relative to the ratchet geometry as those described above. The resulting acceleration, though not yet quantified, is noticeably more significant than that which results from one ratchet surface on the underside of the droplet. It can

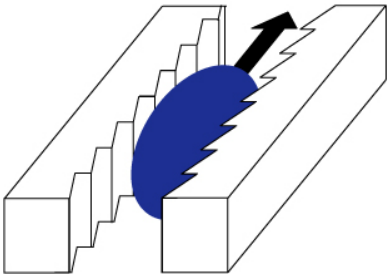

Figure 2.5: A channel with ratchet side walls. In the diagram, the drop of liquid would be observed to move in the direction of the arrow. Also see video at [2].

move slugs of liquid up substantial inclines and becomes stronger as the width of the channel is narrowed. This observation suggests that the role of gravity in the ratchet system is not unique; its function is merely to confine the liquid to the ratchet surface and force an interaction between droplet and ratchet. This type of channel may facilitate the use of a Leidenfrost ratchet mechanism for liquid transport in applications such as microchip cooling [15], or other environments where traditional pumping and/or cooling techniques may have disadvantages.

Chapter 3

Vapor Flow Model

Having now developed an understanding of the basic behavior of the Leidenfrost ratchet system, further physical inquiry requires the development of a working model for the mechanisms of the driving ratchet force. Such a model was initially developed by Benjamín Alemán in 2004 [17]. This chapter will begin by laying out his formulation of the vapor flow model. I will then taylor the model to our droplet system and provide a comparison to initial experimental results.

3.1 Motivation and Initial Considerations for a Vapor Flow Model

As a consequence of being in the Leidenfrost boiling regime, a droplet in our system is separated from the ratchet surface by a thin layer of vapor. It is therefore natural to expect this vapor layer to play an important role in the generation of the ratchet force.

For a film boiling droplet on a *flat* surface, gas escapes via the vapor layer in all horizontal directions equally. When placed on a ratcheted surface, however, the

symmetry of the system is broken, which is assumed to result in a net flow of vapor along one direction relative to the ratchet geometry (see figure 3.1). The model assumes that this flow of vapor tends to pull the droplet along with it by viscous drag, resulting in the observed movement of the droplet.

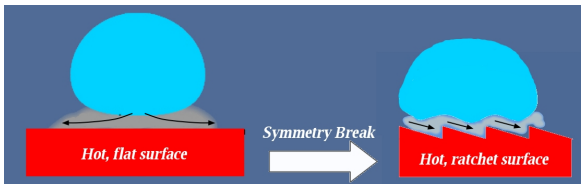

Figure 3.1: A break in symmetry in the ratchet system may lead to directed vapor flow, eventually causing droplet motion. Arrows indicate assumed vapor flow.

3.1.1 Modeling Vapor Flow with a Parallel Plate Geometry

Due to the surface tension of the liquid, the droplet curves around the ratchet geometry in such a way that it is very close to the surface in some areas and relatively far above the surface in others (see figure 3.2). It will be shown in section 3.2.3 that at its closest, the droplet is likely to be at a distance on the order of at most a few tens of microns. As the droplet curves away from the surface, the distance between them rapidly becomes of order $0.1mm$ (the "depth" of one ratchet tooth is $0.3mm$). In order to conserve mass flux across this transition from the proximate region (call it region "1") and the far region ("2"), the velocity of the vapor must decrease by at least an order of magnitude (assuming incompressibility):

$$\rho A_1 v_1 = \rho A_2 v_2$$

$$\frac{v_1}{v_2} \cong 10$$

It is therefore reasonable to concentrate on the areas where ratchet and droplet are in

close proximity and parallel to each other. Adopting this restriction greatly simplifies the study of vapor flow in the ratchet system; it allows the use of a parallel plate geometry for flow within the vapor layer. It is also plausible that outside of these regions, vapor is capable of escaping in such a way as to not affect droplet motion (namely, in a direction transverse to droplet motion).

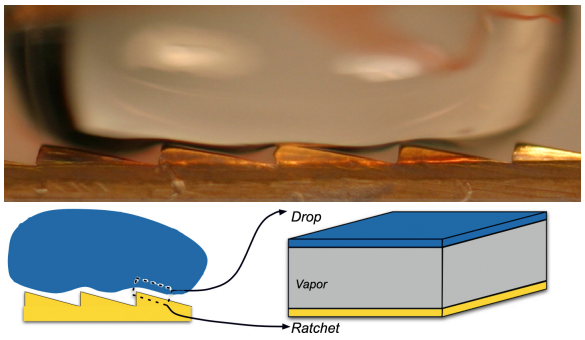

Photo

Illustration

Figure 3.2: Attention is given to those areas where droplet and ratchet form a parallel plate geometry. The upper plate being the drop of liquid and the lower plate being the ratchet surface.

For fluid flow between parallel plates, there are commonly two types of laminar flow. Poiseuille flow arises due to a gradient in pressure along the fluid channel and will result in the driving force in our system. Couette flow is caused by the relative motion of the two plates (it will arise once the droplet is in motion) and will result in a drag force which opposes motion [20]. The next sections go through the mathematical derivation of these two types of flow.

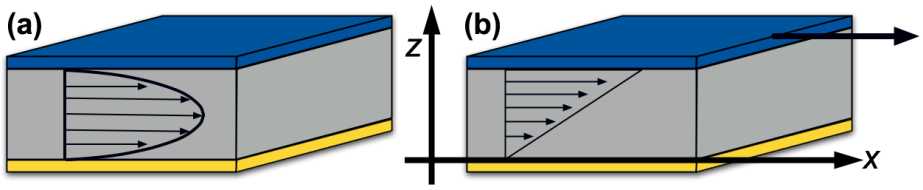

Figure 3.3: Velocity profiles of vapor in Poiseuille **(a)** and Couette **(b)** type flow. The top arrow in **(b)** indicates the movement of the upper plate. Adapted from [20].

3.1.2 Vapor Flow Within Parallel Plate Geometry: Solving the Navier-Stokes Equation

The set of differential equations that describe the motion of a fluid are known as the Navier-Stokes equations [20]. Here, I begin with the equation specific to an incompressible fluid, simplified by the lubrication approximation (see appendix B):

$$-\frac{\partial P}{\partial x} + \eta \frac{\partial^2 v}{\partial z^2} = 0 \tag{3.1}$$

where P is pressure, η is the viscosity the fluid, v is its velocity, and the x and z directions are defined in figure 3.3. To obtain the velocity profile $v(z)$ of the vapor flow in the Leidenfrost ratchet system, we integrate twice and apply the boundary conditions that the vapor at the upper (liquid) and lower (ratchet) plates is stationary relative to the plates themselves.

$$\begin{aligned} \eta \frac{\partial^2 v}{\partial z^2} &= \frac{\partial P}{\partial x} \\ \eta \int\int \frac{\partial^2 v}{\partial z^2}\, dz\, dz &= \int\int \frac{\partial P}{\partial x}\, dz\, dz \\ v(z) &= \frac{1}{2\eta}\frac{\partial P}{\partial x} z^2 + C_1 z + C_2 \end{aligned} \tag{3.2}$$

Since the lower plate represents the surface of a stationary ratchet, the velocity there is zero. Applying $v(0) = 0$:

$$\begin{aligned} v(z)|_{z=0} &= 0 \\ &\Rightarrow \; C_2 = 0 \end{aligned}$$

The upper plate represents the surface of a drop of liquid, whose velocity changes as a function of time. The condition that vapor not move with respect to the droplet surface means that it must have the same velocity as the drop. Applying $v(h) = v_{drop}$:

$$\begin{aligned} v(z)|_{z=h} = v_{drop} &= \frac{1}{2\eta}\frac{\partial P}{\partial x}h^2 + C_1 h \\ \Rightarrow \; C_1 &= \frac{v_{drop}}{h} - \frac{h}{2\eta}\frac{dP}{dx} \end{aligned}$$

The general expression for the velocity profile $v(z)$ now now reads:

$$v(z) = \frac{1}{2\eta}\frac{\partial P}{\partial x}z(z-h) + \frac{v_{drop}}{h}z \tag{3.3}$$

The first term represents a pressure driven Poiseuille type flow while the second represents the drag-inducing Couette type flow. Except in the instance where the droplet is not moving with respect to the ratchet, the typical vapor flow will be a combination of these two basic types. Figure 3.4 shows the velocity profile within the vapor layer for various droplet speeds.

3.1.3 Net Force and Equation of Motion

Now that we have a good idea of how the vapor is flowing in the ratchet system, it is relatively simple to arrive at an expression for the force exerted on the droplet. This force will be due to frictional forces between the droplet surface and parallel layers of the vapor flow. It will be proportional to the area of the drop upon which the vapor interacts; a given vapor flow acting over a larger area results in a greater force. Also, for a given vapor flow $v(z)$, the resulting force will be proportional to the differential $\frac{\partial v(z)}{\partial z}$. A large value for this quantity corresponds to a large difference in velocity between adjacent vapor layers, resulting in a greater frictional force [21]. The resulting force on a droplet is then given by:

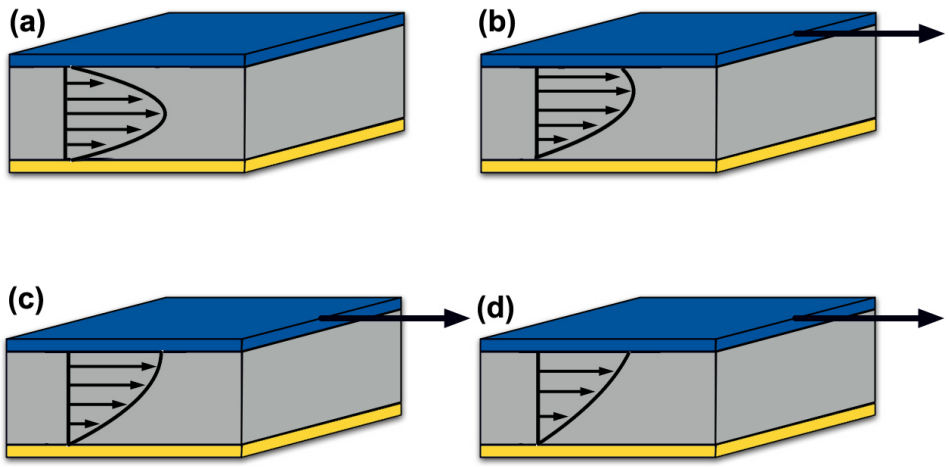

Figure 3.4: Velocity profiles of vapor for varying droplet speeds. **(a)** is at $v_{drop} = 0$, **(b)** is at $v_{drop} = \frac{1}{2}v_{terminal}$, **(c)** at $v_{drop} = v_{terminal}$, and **(d)** at $v_{drop} = 2v_{terminal}$. Note the sign of the gradient (with respect to z) of each at $z = h$. The expression for terminal velocity was obtained from the proceeding treatment of the net force.

$$F_{drop} = -F_{vapor} = -\eta \mathbb{A} \frac{\partial}{\partial z}[v(z)]_{z=h} \tag{3.4}$$

where the constant of proportionality is the viscosity of the vapor. Note the sign convention, if the velocity is *increasing* as the vertical height increases, kinetic energy from the drop goes into frictional forces between vapor layers and the droplet slows down under the influence of a *negative* force (see figure 3.4). Inserting expression 3.3, we obtain

$$F = \left(-\frac{h}{2}\frac{\partial P}{\partial x} - \eta \frac{v_{drop}}{h} \right) \mathbb{A} \cos\theta \tag{3.5}$$

The $\cos\theta$ term has been added to account for the directionality of the ratchet "teeth" (see figure 3.12). This total force exerted on the drop may be interpreted as the sum of two independent forces. A driving "ratchet force" caused by a pressure gradient, and a dissipative "drag force" caused by viscous drag.

Expression 3.5 is still too general a form to be useful in modeling the Leidenfrost ratchet system. All work in the present section up to this point, including the proposal of a vapor flow model and how to apply it, was in place prior to my involvement (largely due to [17], whose contributions are also present to a lesser extent in some of the following sections), my focus has been bridging the gap between theory and experiment. Before proceeding with an actual experimental trial, it is necessary to determine more detailed expressions for:

- The vapor layer thickness h
- The pressure gradient $\frac{\partial P}{\partial x}$
- The area of the droplet $\mathbb{A}$

These parameters will be specific to the Leidenfrost ratchet system, and are the subjects of the proceeding sections.

3.2 Tailoring the Vapor Flow Model to the Leidenfrost Ratchet System

3.2.1 "Contact Area" $\mathbb{A}_c$

The first term that I would like to consider in equation 3.1.3 is the area term $\mathbb{A}$. In the preceding formulation, $\mathbb{A}$ was the area of one "plate" in the specified geometry. The expression applicable to the Leidenfrost ratchet system must therefore take into account only those areas of a droplet where the surface is parallel to the ratchet. In later sections, I will refer to this area as the "effective" area $\mathbb{A}_{eff}$. In order to formulate an expression for this amount of area, I will begin by looking at the more common case of a droplet film boiling on a flat surface, which has been studied in some detail.

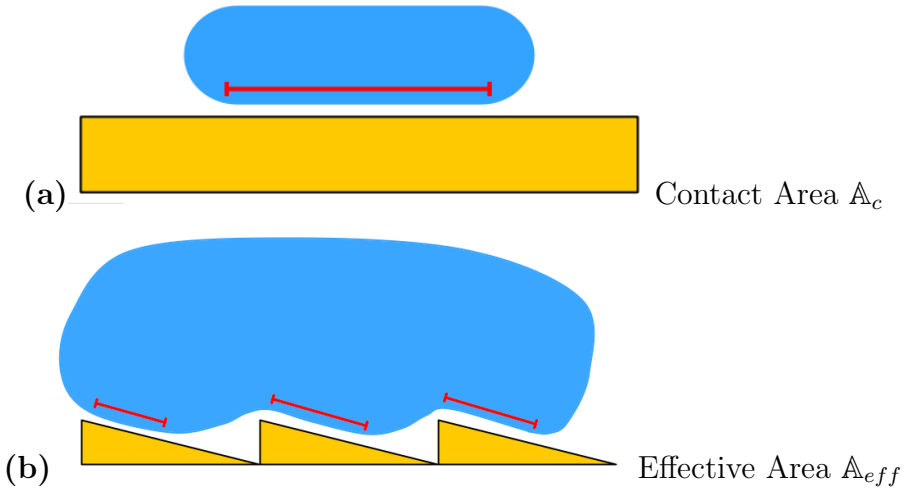

Figure 3.5: The physical quantities "$\mathbb{A}_c$" and "$\mathbb{A}_{eff}$" are illustrated in **(a)** and **(b)** respectively. In each case, the area has been marked with a red line.

There exist in the literature two separate formulations for this area, which is referred to as the "contact area" $\mathbb{A}_c$ of a droplet (somewhat misleading, since a film boiling droplet is not in contact with the substrate). The first is offered by Baumeister *et al.* [22] and is derived from a numerically obtained solution to the *Laplace capillary equation* (which will appear in a later section about the pressure gradient $\frac{\partial P}{\partial x}$), the second is developed by [23, 24] and is based on simple geometry and scaling laws.

Scaling law-obtained expression for contact area.

To a certain extent, film boiling drops of liquid can be regarded as equivalent to droplets placed on a non-wetting surface. Such droplets experience competing forces due to gravity, which tends to flatten them out, and surface tension, which prefers a spherical shape (minimizing surface area). A useful quantity when dealing with this type of interplay between forces is what is known as the "capillary length" κ^{-1}.It is derived by balancing the Laplace pressure (produced by surface tension forces) and the hydrostatic pressure (produced by gravity) for a spherical droplet of radius κ^{-1}:

$$\begin{aligned} \gamma\left(\frac{1}{R}+\frac{1}{R}\right) &= \rho g h \\ 2\gamma\kappa &= 2\rho g \kappa^{-1} \\ \kappa^{-1} &\equiv \sqrt{\frac{\gamma}{\rho g}} \end{aligned} \tag{3.6}$$

where γ is the surface tension, ρ is the density of the liquid, and g is the acceleration due to gravity. The capillary length can be thought of as the length scale beyond which the influence of gravity becomes important [25]. For example, if a normally flat surface is pertubed in such a way as shown in figure 3.6, it returns to its flat geometry after a horizontal distance roughly equal to one capillary length.

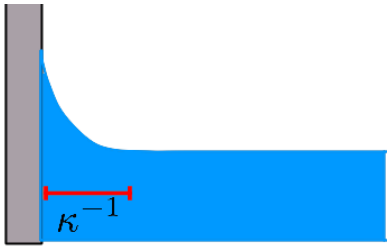

Figure 3.6: Liquid displaced by an object returns horizontal in a distance of one capillary length. Adapted from [25].

In formulating an expression for $\mathbb{A}_c$, [23, 24] distinguish two separate volume regimes which are characterized by droplet shape. For droplets whose volumetric radius R (given by $V = \frac{4}{3}\pi R^3$) is smaller than one capillary length, the shape is considered roughly spherical with a flattened bottom (see figure 3.7).

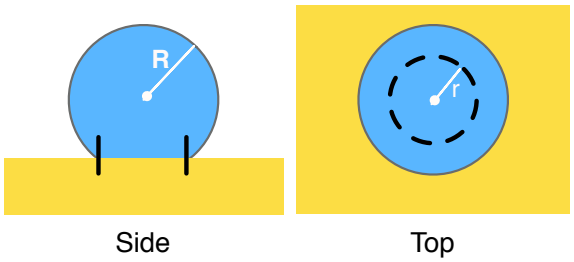

Figure 3.7: Top and side view of a small droplet. The marked area is where the droplet is in "contact" with the surface. R and r are also illustrated.

In order to determine how the "contact radius" r scales with volume, I examine the geometry of figure 3.8:

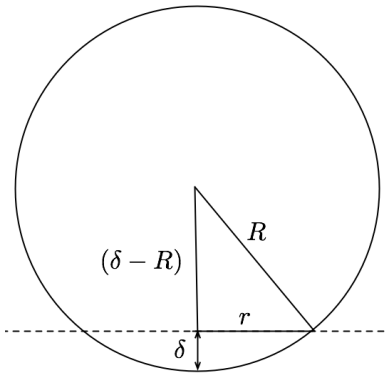

Figure 3.8: Geometry considered for drops with $R < \kappa^{-1}$. The center of mass is lowered an amount δ against a flat surface (dashed line), deforming the spherical shape.

This figure depicts a droplet whose center of mass has been lowered by an amount δ against a flat surface. Following the derivation in [24], the energy cost to do this is approximated by:

$$\Delta E \propto \gamma\delta^2 - \rho g R^3 \delta \tag{3.7}$$

Minimizing the energy, a scaling law for δ is obtained.

$$\begin{aligned} \gamma\delta^2 &\propto \rho g R^3 \delta \\ \delta &\propto \frac{\rho g}{\gamma} R^3 \\ \delta &\propto \kappa^2 R^3 \end{aligned} \tag{3.8}$$

Examining the geometry of figure 3.8, we see that r and δ can be related to R:

$$\begin{aligned} (R-\delta)^2 + r^2 &= R^2 \\ r^2 &= 2R\delta - \delta^2 \end{aligned}$$

So for very small values of δ,

$$r^2 \approx 2R\delta \tag{3.9}$$

into which we can insert equation 3.8 to obtain

$$r \propto R^2\kappa \tag{3.10}$$

This relation is verified by [24], where the numerical constant is found to be about 0.9.

Once a droplet's radius exceeds one capillary length, its shape is more accurately described as a "puddle" than a sphere (see figure 3.9). The height of such a puddle is constrained to $2\kappa^{-1}$ by surface tension and hydrostatic forces (2γ and $.5\rho g h$ by length, respectively) [23]. Any volume added to the drop will increase the puddle

radius, while the height remains fixed at $2\kappa^{-1}$. A scaling law for r is obtained by relating the spherical volume to a cylindrical volume of radius r:

$$\begin{aligned} V &\propto R^3 \\ V &\propto \kappa^{-1} r^2 \\ r &\propto R^{\frac{3}{2}} \kappa^{\frac{1}{2}} \end{aligned} \tag{3.11}$$

The physical quantity termed "contact area" is defined by $\mathbb{A}_c \equiv \pi r^2$. Using the above expressions for r, we obtain:

$$\mathbb{A}_c = \begin{cases} .81\pi R^4 \kappa^2 & \text{if } R \leq \kappa^{-1} \\ .81\pi R^3 \kappa & \text{if } R \geq \kappa^{-1} \end{cases} \tag{3.12}$$

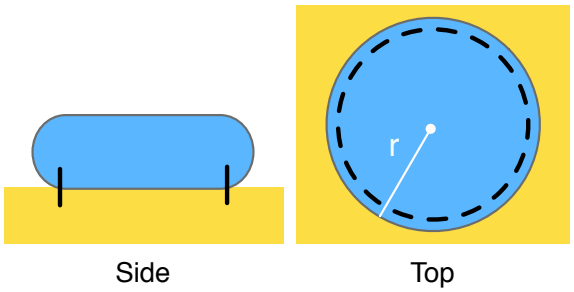

Figure 3.9: Top and side view of a large droplet. Although the actual contact area of the drop is that which is indicated in the figure, the formulation for $\mathbb{A}_c$ includes the extra area outside this radius, as shown.

Using water as an example, this area is plotted below for illustrative purposes. In the figure, I have included a shaded region where the two curves meet. This is as a reminder that they represent the *asymptotic* behavior of the contact area and should be connected by a smooth transition from one to the other.

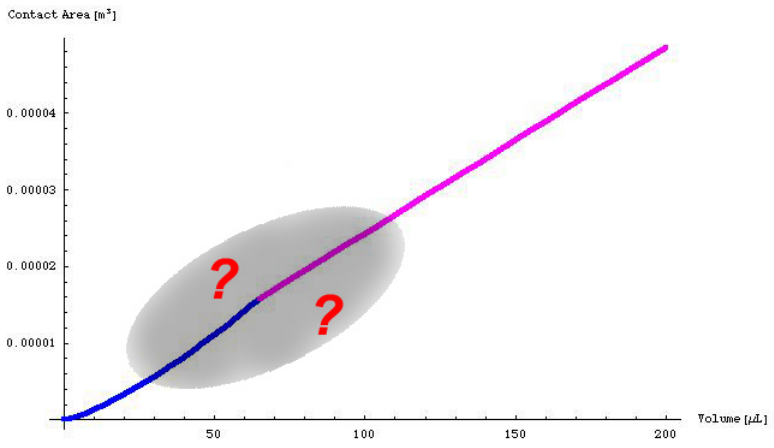

Figure 3.10: Contact area $\mathbb{A}_c$ for water. For drops with $R < \kappa^{-1}$, the area grows with volume as $V^{\frac{4}{3}}$. For drops with $R > \kappa^{-1}$, the area grows linearly with volume. The shaded region indicates the fact that the two curves do not connect directly; they are only accurate for *asymptotic* regions of the graph.

Baumeister's expression for contact area.

A consequence of a liquid's surface tension is that there is typically a difference in pressure between a droplet's interior and the external environment [25]. This is known as the *Laplace pressure*, and was mentioned in the previous discussion.

This difference in pressure is given by the *Laplace capillary equation*:

$$P_{in} - P_{out} = \gamma \left(\frac{1}{R_x} + \frac{1}{R_y} \right) \tag{3.13}$$

where R_x and R_y represent the radii of curvature along two different axes. What the equation says is that if the pressure across a liquid's surface increases, the "curvature" $\frac{1}{R}$ must also increase by the same amount. For example, the capillary equation for a sphere is

$$\Delta P = \frac{2\gamma}{R}$$

$$(\Delta P)R = 2\gamma$$

The product $(\Delta P)R$ is a constant. Equation 3.13 will be revisited in section 3.2.4 in order to determine the pressure gradient $\frac{\partial P}{\partial x}$ in the ratchet system. For the present discussion, it is sufficient to recognize that this over/under pressure dictates the equilibrium shape adopted by a drop of liquid and can therefore be used to determine the contact area $\mathbb{A}_c$. The approach taken by [22] was to numerically solve the equation for film boiling droplets on a flat surface, obtaining an expression for $\mathbb{A}_c$.

Droplet volume is first non-dimensionalized by defining $V^* \equiv \kappa^3 V$. The shape adopted by droplets is shown to fall into three regimes determined by the dependence of droplet thickness on liquid volume. The three corresponding expressions for the contact area are given as:

$$\mathbb{A}_c = \begin{cases} 1.5\left(\frac{3\pi}{4}\right)^{2/3} V^{2/3} & \text{if } V^* \leq 0.8 \\ 1.25\kappa^{1/2} V^{5/6} & \text{if } 0.8 \leq V^* \leq 155 \\ 0.54\kappa V & \text{if } V^* > 155 \end{cases} \tag{3.14}$$

Examining these equations, we see that for very small and very large droplets, the contact area closely matches the expressions derived previously (the expressions for large drops are *identical* up to a constant factor). The middle equation in 3.14 effectively "patches together" the asymptotic expressions. It just happens to be that droplets in our experiments typically fall into this transition range (see table 3.1).

Because the expressions derived previously from scaling laws are really only good approximations for very large and very small volumes, it is reasonable to expect equation 3.14 to more accurately describe our ratchet system. Figure 3.11 shows equations 3.12 and 3.14 for water drops over a volume range typical of experiments

Volume corresponding to:	$V^* = 0.8$	$V^* = 155$
Water	$12.5\mu l$	$2430\mu l$
Ethanol	$3.28\mu l$	$635\mu l$
R-134a	$0.98\mu l$	$190\mu l$

Table 3.1: Volume limits for the validity of equation 3.14.

for the Leidenfrost ratchet system.

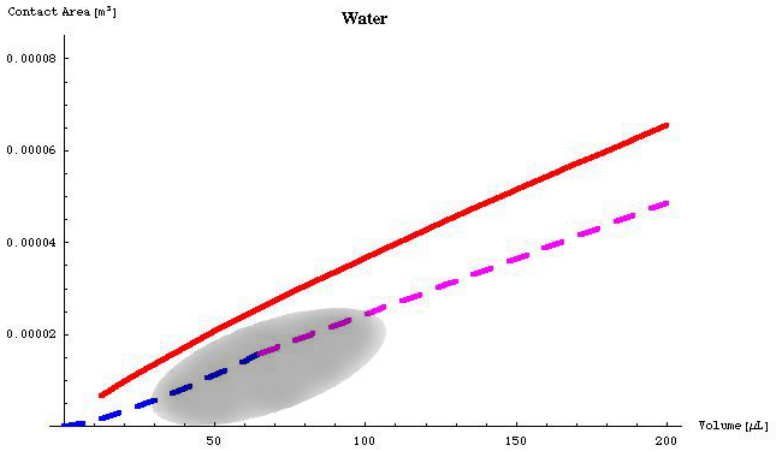

Figure 3.11: Contact area $\mathbb{A}_c$ for water. The solid line represents equation 3.14 and is valid at all points in the range shown, while the dashed equation represents equation 3.12. Typical experiments run over the volume range $\sim 10 - 200\mu l$.

Although we now have some likely expressions for $\mathbb{A}_c$, we recall that what we need is some fraction of this area $\mathbb{A}_{eff}$ that will be specific to droplets on a ratchet surface. This area will vary from $\mathbb{A}_c$ not only because of the shape of the substrate, but also due to the fact that droplets in the ratchet system tend to be "stretched" along the direction of the ratchet force (destroying the circular shape held by a droplet on a flat surface). Accounting for the ratchet shape will be the subject of the next section.

3.2.2 "Contact Length" l and Effective Area $\mathbb{A}_{eff.}$

Because the area term in equation 3.1.3 represents only the area of the droplet that is parallel to the ratchet surface, the contact area $\mathbb{A}_c$ needs to be corrected in order to be applicable to the Leidenfrost ratchet system. The fraction of this area that results in the ratchet force will be referred to as the "effective area" $\mathbb{A}_{eff}$ and must be measured directly. I begin by considering the shape of the droplet and defining a few dimensions as shown in figure 3.12.

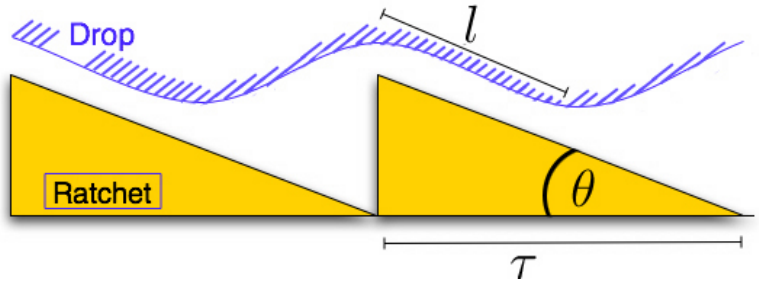

Figure 3.12: Diagram of droplet shape which is adapted from actual photographs (e.g., as in figure 3.13). In the figure, $\tau = 1.5mm$ is the period length and l is the length of droplet surface that is parallel to the ratchet slope, which is approximated in experimental treatments as the distance between a local maximum and the next local minimum. Ratchet depth is $0.3mm$ and $\theta = 11.31°$.

As illustrated in the figure, every horizontal distance of period length τ has associated with it an amount of liquid surface l that is approximately parallel to the ratchet slope. Since the expression for $\mathbb{A}_c$ also pertains to a horizontal area, I define the "effective area" to be this fraction of the total contact area: $\mathbb{A}_{eff} \equiv \frac{l}{\tau}\mathbb{A}_c$. It is not immediately obvious that his would constitute a good approximation for $\mathbb{A}_{eff}$ for a stationary drop. For a moving droplet, however, there will be a time averaging of this area as the droplet moves from one ratchet tooth to another. The assumption would be pretty good for droplets covering at least three full period lengths, getting better as volume increases.

In order to measure this value, high resolution still photographs were taken of a drop of liquid on the ratchet surface large enough to cover multiple period lengths. This

is to ensure that the drop has adopted a general shape. For convenience, as well as objectivity, we define l to be the distance between a local maximum and the next local minimum. Using known ratchet dimensions as a scale, the characteristic length l is measured for ethanol and water.

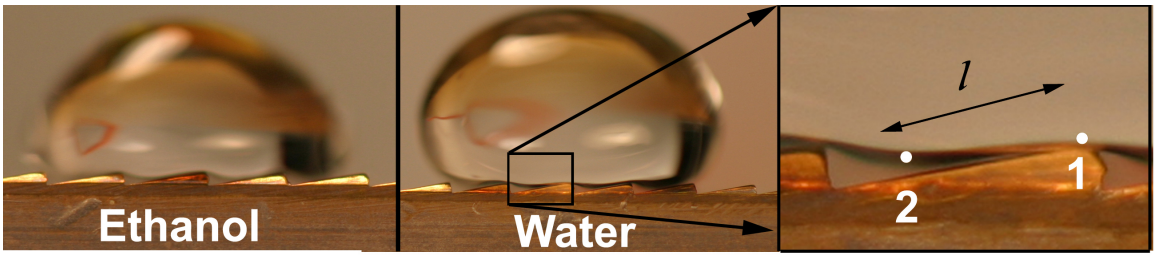

Figure 3.13: Images used to measure parameter l. Ratchet period length $\tau = 1.5mm$ is used as a scale. Volumes are around $60\mu l$, with temperatures about twenty degrees above each liquid's change over to the high temperature regime. We choose the local minima/maxima for points 1 and 2 in an attempt to be objective with visual data.

The measured values for $\frac{l}{\tau}$ are collected in table 3.2 below.

	$\frac{l}{\tau}$
Ethanol	0.70
Water	0.60
R-134a	0.76

Table 3.2: Measured values for $\frac{l}{\tau}$ for ethanol and water.

It should be noted that this procedure must be carried out at temperatures corresponding to those which experiments are to be carried out. This is because the surface tension lowers with an increase in temperature, affecting the measurement. It is also important that the droplet be large enough to cover multiple period lengths in order to avoid the influence of edge affects, where the droplet curves upward.

3.2.3 Vapor Layer Thickness h

I now turn my attention to perhaps the most difficult term in equation 3.1.3 to obtain. Measuring this quantity directly has been done for droplets on a flat surface by [23], and is found to typically be on the order of $10 - 100\mu m$. This was accomplished by studying the diffraction pattern produced by directing a laser through the vapor layer. Such an experiment for a droplet on a ratchet surface is currently underway by our group, but until data is available, I must use a more indirect approach to measure the value of h for droplets in the Leidenfrost ratchet system.

Note that the drag force depends on h:

$$\begin{aligned} F_{drag} = -\beta v_{drop} &= -\eta \frac{v_{drop}}{h} \mathbb{A}_{eff} \\ m\frac{\beta}{m} &= \frac{\eta}{h} \mathbb{A}_{eff} \end{aligned} \tag{3.15}$$

Solving for h, one obtains:

$$\begin{aligned} h &= \frac{\eta}{(\frac{\beta}{m})} \frac{\mathbb{A}_{eff}}{m} \\ &= \frac{\eta}{(\frac{\beta}{m})} \frac{\mathbb{A}_{eff}}{\rho V} \cos\theta \end{aligned} \tag{3.16}$$

Here, $\cos\theta$ has once again been used to correct for the directionality of the drop. $\frac{\beta}{m}$ is one of the fit parameters obtainable from fit equation 2.2, ρ is the liquid's mass density, and V is the volume of the drop. Using this formulation, it is a simple matter to infer the value for h from experimental data for $\frac{\beta}{m}$.

3.2.4 Droplet Curvature and Pressure Gradient $\frac{dP}{dx}$

As mentioned in section 3.2.1, the surface of a drop of liquid has a curvature that is directly related to a difference between internal and external pressure. For every point on the surface, this over/under pressure is given by the *Laplace capillary equation* [25]:

$$P_{in} - P_{out} = \Delta P = \gamma \left(\frac{1}{R_x} - \frac{1}{R_y} \right) \tag{3.17}$$

Here P is pressure, γ is the surface tension of the liquid, and R and R' are the radii of curvature along the two dimensions of the surface (on the surface of a sphere, both radii would be equal and positive, while for a saddle, one would be positive, the other negative).

In order to employ this equation to obtain the pressure gradient $\frac{\partial P}{\partial x}$ in the Leidenfrost ratchet system, I first make a few observations. Although equation 3.17 involves two radii of curvature, a droplet on a ratchet surface curves only in one dimension (excluding the outer edges). A droplet curves around the ratchet's profile, as shown in figure 3.14, but is flat across its width. This is equivalent to having an infinite radius of curvature (in one dimension) at all points away from the outer edges. As $R_y \longrightarrow \infty$, $\frac{1}{R_y} \longrightarrow 0$ and equation 3.17 simplifies to $\Delta P = \frac{\gamma}{R}$.

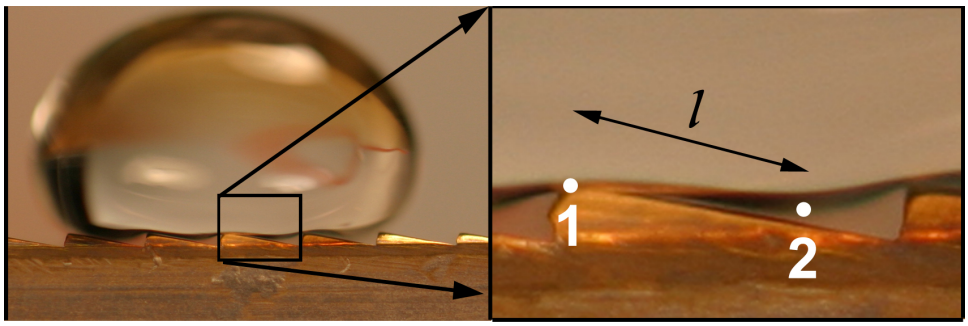

Figure 3.14: Diagram of droplet curvature. The surface of the droplet is seen to curve around the ratchet at points 1 and 2, while remaining flat in the direction perpendicular to the plane of the page.

If I now make the assumption that the internal pressure of the drop is constant, the difference in pressure between points 1 and 2 (defined as the distance between a local maximum and the next minimum, see figure 3.14) is easily obtained:

$$\begin{aligned} P_1^{in} - P_1^{out} &= \gamma\left(\frac{1}{R_1}\right) \\ P_2^{in} - P_2^{out} &= \gamma\left(\frac{1}{R_2}\right) \\ P_1^{out} - P_2^{out} = \Delta P &= \gamma\left(\frac{1}{R_2} - \frac{1}{R_1}\right) \end{aligned} \tag{3.18}$$

Once again labeling l as the distance over which this occurs, the pressure gradient $\frac{\partial P}{\partial x}$ between points 1 & 2 is roughly given by:

$$\frac{\partial P}{\partial x} \approx \frac{\Delta P}{\Delta x} = \frac{\gamma}{l}\left(\frac{1}{R_2} - \frac{1}{R_1}\right) \tag{3.19}$$

By measuring the radii of curvature at these two points (see Appendix D), the pressure gradient, which is responsible for the ratchet force, can be calculated and inserted into equation 3.5.

3.3 Experimental Verification

The data acquired through fit equation 2.2 gives numerical values for the acceleration a due to the ratchet force, and the drag term $\frac{\beta}{m}$. In order to test the idea of $F_{ratchet}$ being produced by the mechanisms of the vapor flow model, I would like to compare the predicted dependence $a(V) \equiv \frac{F_{ratchet}}{m}$ from the model to experimentally measured values for a over a range of volumes V. I begin with the $F_{ratchet}$ component of equation 3.5 and solve for a using Newton's second law:

$$\begin{aligned} F_{ratchet} = ma &= -\frac{h}{2}\frac{\partial P}{\partial x}\mathbb{A} \\ a &= -\frac{h}{2}\frac{\partial P}{\partial x}\frac{\mathbb{A}}{m} \\ a &= -\frac{h}{2}\frac{\partial P}{\partial x}\frac{\mathbb{A}}{\rho V} \end{aligned} \tag{3.20}$$

I now set $\mathbb{A} = \mathbb{A}_{eff}$ and insert equations 3.14 and 3.19:

$$\begin{aligned} a(V) &= -\frac{h}{2}\frac{\gamma}{l}\left(\frac{1}{R_2} - \frac{1}{R_1}\right)\frac{1}{\rho V}\frac{l}{\tau}\frac{5}{4}\left(\frac{\gamma}{\rho g}\right)^{-\frac{1}{4}} V^{\frac{5}{6}}\cos\theta \\ &= \frac{h}{2\tau}\left(\frac{\gamma^3 g}{\rho^3}\right)^{\frac{1}{4}}\left(\frac{1}{R_1} - \frac{1}{R_2}\right)V^{-\frac{1}{6}}\cos\theta \end{aligned} \tag{3.21}$$

Before comparing this equation to experimental data, it is still necessary to insert an experimentally determined value for h. I therefore use equation 3.16, along with experimental values for $\frac{\beta}{m}$ and $\frac{l}{\tau}$ to see how the value for h varies over a range of volumes. This is summarized in figure 3.15.

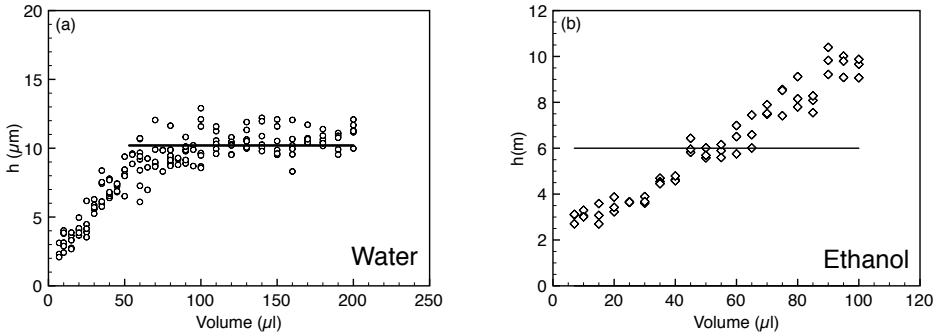

Figure 3.15: Experimentally determined values of h, using the expression for $\mathbb{A}_c$ that scales as $V^{5/6}$, for water **(a)** at $460°C$ and ethanol **(b)** at $300°C$. The horizontal line indicates the average value in the $50-200\mu l$ range for water and over all volumes for ethanol.

Equation 3.21 and figure 3.15 represent how acceleration is to be calculated if we use the formulation of $\mathbb{A}_c$ given by [22]. I also want to consider the acceleration that results from using the expressions for $\mathbb{A}_c$ derived in section 3.2.1 as outlined in [23, 24]. Inserting equation 3.12, an alternate expression for $a(V)$ is derived:

$$a(V) = \begin{cases} (.81\pi)\left(\frac{3}{4\pi}\right)^{4/3}\frac{h}{2\tau}\cos\theta\left(\frac{1}{R_1}-\frac{1}{R_2}\right)gV^{1/3} & \text{if } R \leq \kappa^{-1} \\ \\ (.81)\frac{3h}{8\tau}\left(\frac{1}{R_1}-\frac{1}{R_2}\right)\sqrt{\frac{\gamma g}{\rho}}\cos\theta & \text{if } R \geq \kappa^{-1} \end{cases} \tag{3.22}$$

The corresponding calculation of vapor layer thickness h is also performed using equation 3.12 into the equation for $h(V)$ (3.16) and is shown in figure 3.16.

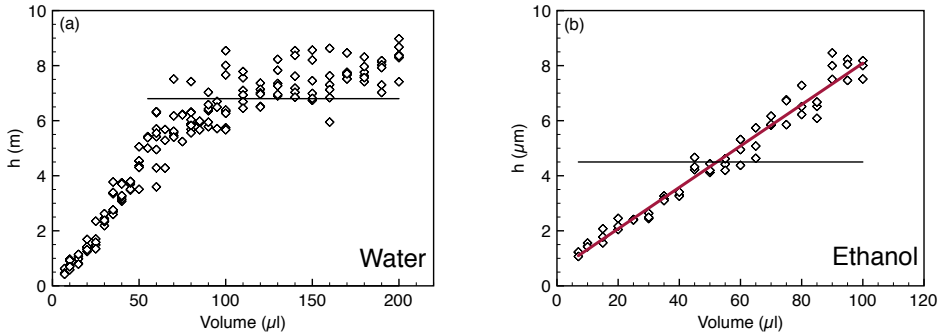

Figure 3.16: Experimentally determined values of h, using the scaling-law expression for $\mathbb{A}_c$, for water **(a)** at $460°C$ and ethanol **(b)** at $300°C$. For water, the horizontal line indicates the average value in the $50 - 200\mu l$ range. For ethanol, the horizontal line is an average over all volumes and the red line is a linear fit to the data.

I note that beyond $50\mu l$, the value for h becomes roughly constant for water. Because experimental data for acceleration generally shows significant scatter for volumes below $50\mu l$, I will use the average value for h in the $V > 50\mu l$ range while realizing that the acceleration dependence $a(V)$ will not be valid for $V < 50\mu l$. Using the value $h \approx 10.2\mu m$ in equation 3.20, I can now compare it to experimentally measured values for a as show in figure 3.17 below. As for the ethanol data, using the average is not justified by the experimental data. I therefore use both a linear fit to the data and the average value for h in the comparison to theory.

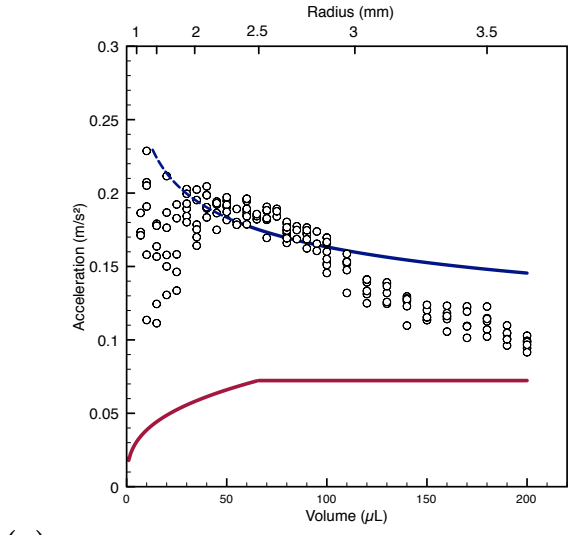

(a)

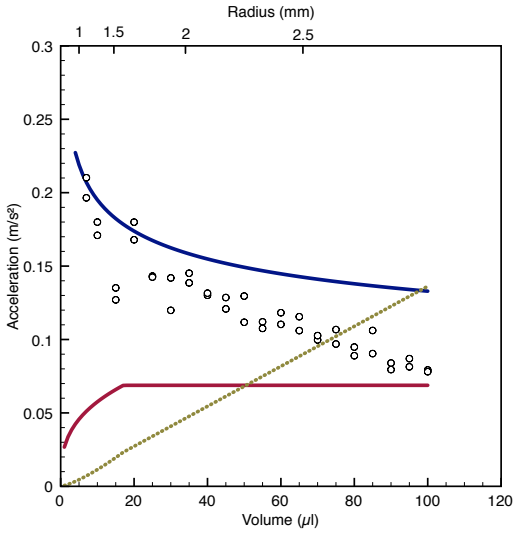

(b)

Figure 3.17: Acceleration as a function of volume for water **(a)** at $460°C$ and ethanol **(b)** at $300°C$. The upper curve represents acceleration determined using contact area from [22] (equation 3.21) with the corresponding experimentally calculated value for h. The dashed segment of this curve indicates the model's invalidity in that region, where considerations for l/τ, h, and $\mathbb{A}_c$ are inadequate. Lower curves are for acceleration determined using the scaling-law derived contact area from [23, 24] (equation 3.22), with the red curves using the average calculated value for h and the dashed line using a linear fit for h, as shown in figures 3.15 and 3.16.

Chapter 4

Conclusive Remarks

The measured values for acceleration due to $F_{ratchet}$ in the Leidenfrost ratchet system agree quantitatively with a vapor flow model which uses the expression for contact area that scales as $V^{5/6}$. As expected, contact area equation 3.14 seems to also *qualitatively* describe droplets in the typical volume range spanned by experiment more accurately. Error introduced into the model is mainly due to measurements of $\frac{l}{\tau}$, R_1, R_2, and h. The first three depend on the quality of photograph attainable, as well as human error. These errors will be difficult to reduce unless an alternative method of measurement is found. Data for h, however, may be improved significantly through the method of measurement offered in [23, 24], which is currently in progress by our group. It is also likely that there are other more complicated effects that must be factored into the present thinking, such as droplet oscillations, thermo-capillary flow, and stretching of droplets that is observed in the ratchet system.

In order to explore applications such as microchip cooling [15], work needs to be done in order to determine how the effect may be scaled down to useful sizes. Specifically, varying ratchet dimensions such as depth, period length, and slope will be important to obtain optimal results. The type of liquid will also be important since the surface tension will likely need to be low for smaller ratchet dimensions. Of particular interest for applications could be ratchet channels such as that illustrated in figure 2.5 and shown online at [2]. Because it is likely important for vapor to escape the ratchet

geometry at some point, a completely closed channel may not work properly and different channel designs should be explored. As with many new and interesting phenomena, novel uses of the Leidenfrost ratchet may arise in unexpected places.

Appendix A

Experimental Procedures

A.1 Cleaning Protocol

To begin with, after a ratchet exits the machine shop and comes into our possession, special care is taken in order to avoid touching the ratchet surface. This prevents the introduction of dirts and oils, which could later be burned onto the surface. Because of the often large differences in temperature at which experiments are performed for different liquids, each liquid used to gather experimental data has it own ratchet. These are never heated to a temperature beyond that at which experiments are performed. As illustrated in section 2.2, the cleanliness (or rather, method of cleaning) of the ratchet is capable of significantly altering droplet behavior (it has even been observed that ratchets with significant material in the "teeth" can completely reverse the direction of ratchet motion).

Prior to an experimental run, the brass ratchet to be used goes through an established cleaning protocol in order to ensure reproducible conditions. The first step is to polish the ratchet with commercial brass polish (Wright Keane, New Hampshire) and Kimwipes. Special attention is given to ratchet crevices to ensure that all residues are removed. The ratchet is then rinsed with de-ionized water. At this point, the cleaning procedure is complete for those data points indicated by crosses in figure

2.3, which were obtained prior to the establishment of a more rigorous procedure. All other data points, however, were collected after the ratchet underwent the following additional procedures. These were initiated in order to better control ratchet surface properties.

The polished ratchet is placed in a beaker containing acetone and sonicated for five minutes at room temperature. Upon removal, the ratchet is rinsed with and then placed into isopropyl alcohol, where it is sonicated for three minutes. Finally, the process is repeated using methanol, sonicating for an additional three minutes. The ratchet is then dried using nitrogen gas, completing the cleaning procedure.

A.2 Data Collection

In order to gather data for the velocity evolution of a drop, which can be used in fit equation 2.2, a recently cleaned ratchet is placed onto a hot plate, which rests on a leveling platform. The thickness of the ratchet substrate is $\approx 1.2cm$ Temperature was measured by inserting thermocouple probes into small holes drilled into the side of the ratchet approximately $5mm$ from the top surface and $2.5cm$ into the side. Once hot enough for film boiling to occur, droplets are deposited on a flat brass plate in order to adjust the surface until it is level. Properly leveled, the ratchet is filmed from above by a digital video camera, which feeds video onto a computer. Droplets are given an initial velocity by sending them down an incline in the direction opposite that of the ratchet force (see figure A.1). Such a droplet will slow to a stop, reverse direction, and return to the preferred end of the ratchet.

Video clips of droplet motion are analyzed with video tracking software Videopoint (Lenox, MA). For each frame of a droplet's motion on the ratchet, position data is recorded. This position data is used to calculate velocity, which is averaged over three data points. An example of data is shown in figure A.2 in order to specify calculation methods. This averaged velocity data can be fit to equation 2.2 as shown in figure 2.1.

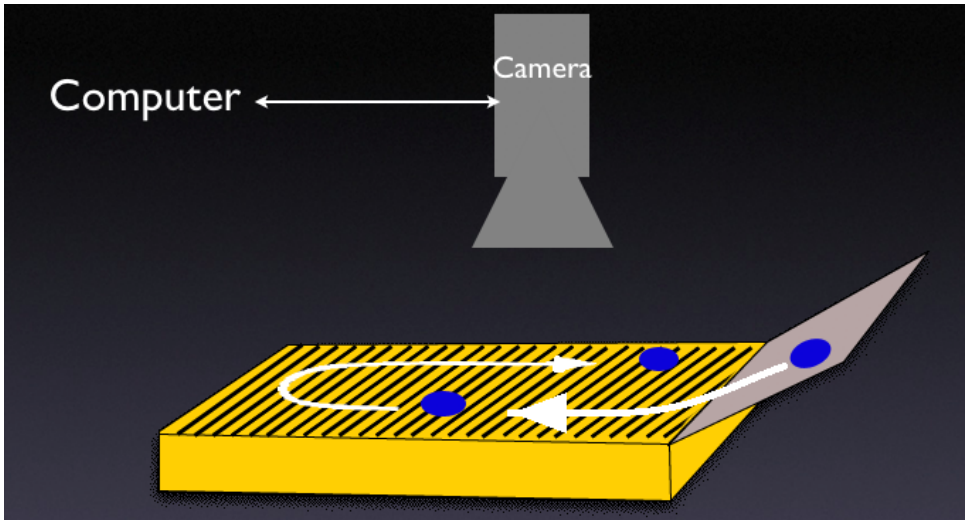

Figure A.1: Experimental setup.

Time	s1 position	s1 velocity	s1 velocity average
0	0.1096		
0.03333333	0.1015	-0.243	
0.06666667	0.09412	-0.2214	-0.2141
0.1	0.08819	-0.1779	-0.1898
0.13333333	0.08252	-0.1701	-0.1637
0.16666667	0.07775	-0.1431	-0.1534
0.2	0.07285	-0.147	-0.138
0.23333333	0.06872	-0.1239	-0.1277
0.26666667	0.06498	-0.1122	-0.1109
0.3	0.06176	-0.0966	-0.1005

Figure A.2: Part of a typical table of values used to calculate droplet velocity. Time is taken to step forward at the frame rate of $\frac{1}{30}s$. Position data in column two is obtained via direct measurement from the video data. Velocity (column 3) is calculated by taking the difference of the prior and current position and dividing by time elapsed. The three point average of velocity (column 4) is calculated as the average of the previous, current, and next cells of column 3.

When carrying out an experiment, it is important to keep a few things in mind. First, the ramp angle should be adjusted periodically so that there is enough initial velocity for the droplet's motion to cover the entire length of the ratchet (while remaining on camera). This ensures the maximum number of data points to use in fit equation 2.2, giving a better measurement of the fit parameters. Also, the transition from ramp to ratchet should be made as smooth as possible to prevent droplets from breaking apart on impact. Experimenting with lighting will give a better contrast of the droplet on the ratchet, making tracking easier.

Appendix B

The Lubrication Approximation

In order to simplify the Navier-Stokes equation to a one-dimensional equation that is linear in v, I invoke the "lubrication approximation" (as well as assuming incompressibility) [25]. This derivation will follow that of [26]. For a fluid, Newton's second law reads as:

$$\vec{f} = \rho \frac{d\vec{v}}{dt} + \rho \vec{v} \cdot \nabla \vec{v} \tag{B.1}$$

where $\vec{f}$ is the force acting on an element of volume, ρ is the mass density, and $\vec{v}$ is the velocity of the element of volume. The additional term on the right takes into account the possibility of $\vec{v}$ field changing overall, in addition to with time [26]. For an incompressible fluid, there is the additional condition $\nabla \cdot \vec{v} = 0$. There are two types of forces present within a fluid, one from a pressure gradient and another from viscosity. Equating the sum of these two forces to the form of Newton's law above, we obtain:

$$\rho \frac{d\vec{v}}{dt} + \rho \vec{v} \cdot \nabla \vec{v} = -\nabla P + \eta \nabla^2 \vec{v} \tag{B.2}$$

The above vector equation constitutes three equations, these are the Navier-Stokes equations. The term $\rho\vec{v}\cdot\nabla\vec{v}$ is inertial, it can be neglected for systems with sufficiently small Reynolds numbers, which is simply a ratio of inertial to viscous forces present. From [20], we have

$$\begin{aligned} Re &= \frac{\bar{v}h}{\nu} \\ &= \frac{\bar{v}h\rho_v}{\eta_v} \end{aligned}$$

where $\bar{v}$ is the average velocity of the vapor, h is the height of the vapor layer, and ν is the kinematic viscosity of the vapor, $\nu = \frac{\eta_v}{\rho_v}$. We integrate our expression for $v(z)$ over h in order to determine $\overline{v(z)}$:

$$\begin{aligned} \overline{v(z)} &= \frac{1}{h}\int_0^h \frac{1}{2\eta}\frac{\partial P}{\partial x} z(z-h) \\ &= -\frac{h^2}{12\eta_v}\frac{\triangle P}{\triangle x} \end{aligned}$$

Using equation 3.19 for $\frac{\Delta P}{\Delta x}$, the Reynolds number is

$$Re = \frac{h^3\rho_v}{12\ l\ \eta_v^2}\gamma\left(\frac{1}{R_2} - \frac{1}{R_1}\right) \tag{B.3}$$

Using values from appendix C, as well as our measured values for curvature and l, we calculate the values of Re for our liquids and find that they are indeed much smaller than 1.

	Re
Water Vapor	6.8×10^{-6}
Ethanol Vapor	1.02×10^{-8}

Table B.1: Reynolds numbers for water and ethanol in vapor "channels."

Since all Reynolds numbers of our system are much less than 1, the inertial term in the Navier-Stokes equation can be left out, leaving:

$$\rho\frac{d\vec{v}}{dt} = -\nabla P + \eta\nabla^2\vec{v} \tag{B.4}$$

If we also want *steady-state* solutions for $\vec{v}$, the left hand side must also be zero, leaving:

$$\nabla P = \eta\nabla^2\vec{v} \tag{B.5}$$

which is further simplified for flow in one-dimension:

$$-\frac{\partial P}{\partial x} + \eta\frac{\partial^2 v}{\partial z^2} = 0 \tag{B.6}$$

This is the equation used to approximate vapor flow within our ratchet system.

Appendix C

Physical Properties

C.1 Liquid Properties

T (K)	T (°C)	ρ $\left(\frac{kg}{m^3}\right)$	γ $\left(\frac{N}{m}\right)$
313.15	40	772.01	-
323.15	50	763	19.89×10^{-3}
340	66.85	-	18.6×10^{-3}
360	86.85	-	16.7×10^{-3}

Table C.1: Properties of Ethanol liquid (B.P. = 78.5°C) (Reference: [27], [28] 15-43, 6-150)

T (K)	T (°C)	ρ $\left(\frac{kg}{m^3}\right)$	γ $\left(\frac{N}{m}\right)$
372.78	99.63	958.63	–
373.15	100	–	58.91×10^{-3}

Table C.2: Properties of liquid water at boiling point (Reference: [28] 6-13, 6-150)

According to [28], temperature dependence of volume is described by cubic expansion coefficient α ($^\circ C^{-1}$). For ethanol at $70^\circ C$, $\alpha = 1.67 \times 10^{-3}$.

$$\alpha = \frac{1}{V}\left(\frac{dV}{dT}\right)_P \tag{C.1}$$

T (K)	T (°C)	$\rho\ \left(\frac{kg}{m^3}\right)$	$\gamma\ \left(\frac{N}{m}\right)$
247.07	-26.08	1376.6	15.54×10^{-3}

Table C.3: Properties of liquid R-134a. (Reference: [27], 2.71)

$$\alpha \cdot V \cdot (dT)_P = (dV)_P \tag{C.2}$$

In terms of density:

$$\rho = \frac{m}{V} \tag{C.3}$$
$$d\rho = -\frac{m}{V^2}\, dV \tag{C.4}$$
$$= -\frac{m}{V^2}\alpha V (dT)_P \tag{C.5}$$
$$= -\frac{m}{V}\alpha (dT)_P \tag{C.6}$$
$$= -\rho\alpha (dT)_P \tag{C.7}$$
$$\rho_f = \rho_i(1 - \alpha dT) \tag{C.8}$$

So if we take the initial temperature to be $50°C$ with a density of 763 $\left(\frac{N}{m}\right)$, the density at the boiling point $78.5°C$ becomes:

$$\rho = 763(1 - 47.6 \times 10^{-3}) \tag{C.9}$$
$$= 727\ \left(\frac{kg}{m^3}\right) \tag{C.10}$$

We also need a better value for surface tension of ethanol at boiling point $78.5°C$. A 2^{nd} degree polynomial is fitted to the three data points from table C.1 and evaluated at the boiling point using Mathematica (Wolfram, USA).

$$\gamma(T) = -0.355562 + 0.00228248x - 3.46782 \times 10^{-6}x^2 \tag{C.11}$$
$$\gamma(351.65) \approx 18.2 \times 10^{-3}\ \left(\frac{N}{m}\right) \tag{C.12}$$

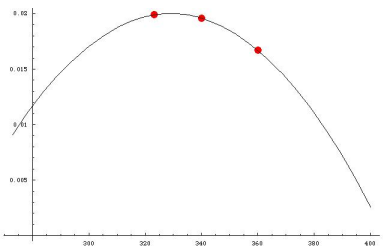

Figure C.1: Fitted data for surface tension of ethanol.

So our table of physical properties now becomes:

	T (C)	T (K)	$\rho\ \left(\frac{kg}{m^3}\right)$	$\gamma\ \left(\frac{N}{m}\right)$
Water	100	373.15	958.63	58.91×10^{-3}
Ethanol	78.5	351.65	727	18.2×10^{-3}
R-134a	-26.08	247.07	1376.6	15.54×10^{-3}

Table C.4: Physical properties of liquids at their boiling points.

C.2 Vapor Properties

For the vapor of these chemicals, we are interested in the viscosity and the density at the average temperature between the boiling point and the ratchet surface. This temperature roughly corresponds to 550K for water,

	$\rho_v\ \left(\frac{kg}{m^3}\right)$	$\eta_v\ (Pa \cdot s)$
Water Vapor	0.36185	19.4×10^{-6}
Ethanol Vapor	.00118	14.5×10^{-6}
R-134a Vapor	4.279 (293.15)	13.2×10^{-6} (317K)

Table C.5: Physical properties of gases at the approximate average of ratchet temperature and boiling points (η for water is taken to be the average of its values at $500K$ and $600K$). Reference: [28] 6-13, 6-201; [29] 56; [30] 11; [31] 5.

Appendix D

Measuring Droplet Curvature

In section 3.2.4, I have shown how it is possible to use the Laplace capillary equation to determine the pressure gradient $\frac{\Delta P}{\Delta x}$ by measuring the radii of curvature at points 1 & 2. To carry out these measurements, I examine the high resolution images used in section 3.2.2.

Each image was imported into a computer data analysis program Phantom (Vision Research, USA), where a coordinate system was established using known ratchet dimensions as a scale. Data points were collected by mouse clicks along the profile of the droplet, recording position coordinates for a number of points along the droplet surface. This position data is imported in Mathematica (Wolfram, USA), where a fourth-order polynomial was fit to the data points immediately surrounding points 1 & 2. The data with fit curves for water is shown in figure D.1 below.

The mathematical definition for the radius of curvature at a point on a curve is given by [32]:

$$r(x) = \frac{(1 + (f'(x))^2)^{\frac{3}{2}}}{f''(x)} \tag{D.1}$$

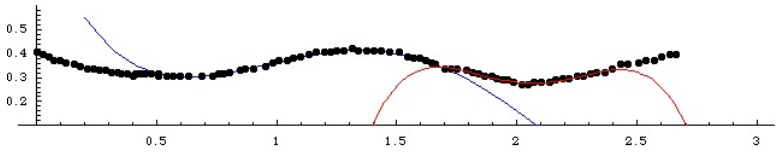

Figure D.1: Curvature data and fit curves for water. The curves shown are fourth-order polynomial fits of the twenty-five data points surrounding the local maximum and minimum.

Which simplifies at maxima/minima (such as points 1 & 2) to:

$$r(x) = \frac{1}{f''(x)} \tag{D.2}$$

Determined in this way, the values of R_1 & R_2 for water and ethanol are gathered in table D.1

	$R_1(mm)$	$R_2(mm)$
Water	-2.19	0.58
Ethanol	-0.21	0.92

Table D.1: Measured values for R_1 & R_2.

Bibliography

[1] J.D. Bernardin and I. Mudawar, J. Heat Transfer, **121** (1999).

[2] See Linke Lab website for illustrative movies of Leidenfrost ratchets in action. URL http://darkwing.uoregon.edu/∼linke/dropletmovies/

[3] F. Brochard, Langmuir **5**, 432 (1989).

[4] M.K. Chaudhury and G.M. Whitesides, Science **256**, 1539 (1992).

[5] K. Ichimura, S.K. Oh, and M. Nakagawa, Science **288**, 1624 (2000).

[6] F. Domingues Dos Santos and T. Ondarcuhu, Phys. Rev. Lett. **75**, 2972 (1995).

[7] J. Bico and D. Quéré, Europhys. Lett. **51**, 546 (2000).

[8] J. Bico and D. Quéré, J. Fluid Mech. **467**, 101 (2002).

[9] Y. Sumino, N. Magome, T. Hamada, and K. Yoshikawa, Phys. Rev. Lett. **94**, 068301 (2005).

[10] J.B. Brzoska, F. Brochard-Wyart, and F. Rondelez, Langmuir **9**, 2220 (1993).

[11] A.A. Darhuber, J.P. Valentino, J.M. Davis, S.M. Troian, and S. Wagner, Appl. Phys. Lett. **82**, 657 (2003).

[12] M.G. Pollack, R.B. Fair, and A.D. Shenderov, Appl. Phys. Lett. **77**, 1725 (2000).

[13] H. Linke, B.J. Alemán, L.D. Melling, M.J. Taormina, M.J. Francis, C.C. Dow-Hygelund, V. Narayanan, R.P. Taylor, and A. Stout, Phys. Rev. Lett **96**, 154502 (2006).

[14] M. Chown, New Scientist **189** 2535 (2006).

[15] F. O'Connell, New York Times, pp. D4 March 21, (2006).

[16] Melling, Laura. "Self-propelled Motion of Film Boiling Droplets on Ratchet-like Surfaces" *(Thesis)*. University of Oregon, Clark Honors College (2003).

[17] Alemán, Benjamín José. "A Vapor Flow Model for Self-propelled Liquid Droplets on Ratchet-like Surfaces" *(Lab Report)*. University of Oregon, Materials Science Institute (2004).

[18] J. Bernardin and I. Mudawar, Journal of Heat Transfer. **121**, pp. 894 (1999).

[19] Gottfried, C.J. Lee, & K.J. Bell, Int. J. Heat Mass Transfer **9**, 1167 (1966).

[20] Panton, Ronald L. *Incompressible Flow*. John Wiley and Sons, Inc. New York, NY. 2^{nd} ed., chapter 7 (1996).

[21] R. Resnick, D. Halliday, and K. Krane. *Physics*, 5^{th} ed., **1**. John Wiley and Sons, Inc. (2002).

[22] K. Baumeister,T.D. Hamill, and G.J. Schoessow. Proceedings of the Third International Heat Transfer Conference, **7** 66 (1966).

[23] A. Biance, C. Clanet, and D. Quéré. Physics of Fluids, **15**, 6 (2003).

[24] P. Aussillous and D. Quéré. "Liquid Marbles," Nature (London) **411**, 924 (2001).

[25] P.G. de Gennes, F. Brochard-Wyart, and D. Quéré. *Capillarity and Wetting Phenomena: Drops, Bubbles, Pearls, and Waves*. Springer-Verlag New York, Inc. New York, (2002).

[26] E.W. Weisstein. *Eric Weisstein's World of Physics*. http://scienceworld.wolfram.com/physics/Navier-StokesEquations.html (2006).

[27] Rohsenow, Warren M. & James P. Hartett & Cho I. Young. *Handbook of Heat Transfer 3rd ed.* McGraw-Hill. New York, (1998)

[28] D.R. Lide, ed. *CRC Handbook of Chemistry and Physics*. CRC Press. Boca Raton, FL. 85^{th} ed., pp. 6-140. (2004)

[29] R.E. Bolz, D.Eng and G..L. Tuve, Sc.D., ed. *CRC Handbook of tables for Applied Engineering Science*. CRC Press. Boca Raton, FL. 2^{nd} ed. (1973).

[30] DuPont. *Thermodynamic Properties of HFC - 134a (1,1,1,2 - tetraflouroethane) Refrigerants*. T-134aSI.

[31] A.P. Fröba, S. Will, and A. Leipertz, "Saturated Liquid Viscosity and Surface Tension of Alternative Refrigerants." Paper presented at the Fourteenth Symposium on Thermophysical Properties, June 25-30, 2000, Boulder, CO, U.S.A.

[32] E.W. Weisstein. *CRC Concise Encyclopedia of Mathematics*. CRC Press, Boca Raton, FL. pp.1508 (1999).